Asian Journal of Control, Vol. 14, No. 2, pp. 413–425, March 2012
Published online 17 January 2011 in Wiley Online Library (wileyonlinelibrary.com) DOI: 10.1002/asjc.340

BATTERY POWER LOSS COMPENSATED FRACTIONAL ORDER SLIDING MODE CONTROL OF A QUADROTOR UAV

Mehmet Önder Efe

ABSTRACT

This work considers the fractional order control of a lightweight quadrotor under loss in the battery voltage. Since the outdoor brushless motors are driven via a pulse width modulation (pwm) scheme, handshaking between the dynamic model and controller is established at the pwm level and this constitutes a major contribution of the paper. The attitude control is achieved via fractional order sliding mode control (FSMC) scheme. Necessary stability considerations are presented and it is seen that FSMC is a good alternative for the control of unmanned aerial vehicles.

Key Words: Fractional order control, quadrotor control, battery voltage loss compensation.

I. INTRODUCTION

The realm of unmanned aerial vehicles (UAVs) is a field of research out of which the number of research reports has an increasing nature. The major reasons fostering this trend are the increase in the computational power in microelectronic circuits and devices, the decrease in the weight of many components and the increase in the efficiency of new batteries. Despite the presence of such facilities, control issues, autonomous flight, image/video capturing, strategic/tactical planning and UAV communications continue to exist as interesting problems of UAV research. Two critical problems of this research field are the design of the controllers and the change in the battery conditions that influence the entire set of functions directly. This paper describes explicitly the problem caused by the loss in the battery voltage and a method to solve it, as well as a novel robust control scheme employing fractional derivatives that has not been implemented for UAVs before.

Manuscript received March 26, 2010; revised July 20, 2010; accepted September 25, 2010.

The author is with the Department of Electrical and Electronics Engineering, Bahçeşehir University, Beşiktaş, İstanbul, Turkey (e-mail: onderefe@gmail.com).

This work was supported by TÜBİTAK, under contract No 107E137.

UAVs have been an inspiration to many researchers for several reasons. Different types of payloads and different types of mission definitions make them different from each other yet in essence, the scope of the applications of UAVs covers the traffic monitoring, border and port security, pipeline security, wildlife documentation, stadium monitoring, search & rescue, coastguarding, meteorologic and agricultural applications, forestry, volcanic activity monitoring, zone monitoring and so on. Depending on the environmental conditions, each one of these applications may require a particularly specified physical UAV configuration. In this study, a quadrotor type UAV is considered. This UAV configuration has been studied several times in the past and it is a vertical takeoff and landing type vehicle capable of carrying lightweight cameras for surveillance. A significant amount of research volume focuses on the design of controllers for quadrotors.

Due to its significant effect on the overall vehicle functionality, the design of controllers, which produce the necessary signals to be sent to the motors, has been the core issue in quadrotor based UAV applications. Several examples of trajectory tracking controllers have been investigated in the literature. A grouped list of the recent volume of works on controller design is given below.

- Classical PID variants, [1, 2]
- Backstepping technique, [3, 4]

- Quadratic optimal control, [5, 6]
- Sliding mode control, [7, 8]
- Quaternion based approaches, [9, 10]
- Feedback linearization, [11]
- Lyapunov methods, [12, 13]
- Vision based control, [14–16]
- Reinforcement learning based control, [7]
- Fuzzy control, [17]

A common point of the approaches considered here is the use of integer order derivatives for continuous time designs and constant valued sampling rate for discrete time designs. An alternative approach is to adopt the fractional order differintegration operators. Although the history of fractional calculus dates back to the 17th century, its applications in systems and control theory are in their infancy. Let $\mathbf{D}:=\frac{\mathrm{d}}{\mathrm{d}t}$ be the integer order differentiation operator. The operator $\mathbf{D}$ in the time domain corresponds to the operator s in the Laplace domain, *i.e.* $\mathscr{L}(\mathbf{D})=s$, and fractional order operator $\mathbf{D}^{\beta}$ with $\beta\in\Re$ creates differentiators of fractional order if $\beta>0$ and integrators of the same type if $\beta<0$, [18–20]. Further, in the Laplace domain this operator has the form s^{β}, and in the frequency domain $(j\omega)^{\beta}$. Having this picture in front of us, it becomes possible to define transfer functions, stability, controllability and observability concepts as well as the concepts of state space formalism, [21]. Clearly the current knowledge about fractional order control for linear systems is much greater than that for nonlinear systems. The novelty introduced here is the application of the reaching law approach of sliding mode control, which is a robust and nonlinear control technique, in fractional order with necessary stability considerations and finite time hitting issues.

Another major issue addressed in this paper is the issue of power loss in batteries. To be more explicit, in simulation, the controller produces the control signals and these are applied to the inputs of the dynamic model, however, the physical system inputs are pulse width modulated signals. Therefore, the controller side and the model side must be separated properly. This paper focuses on such a modeling issue together with the limited power utilities available on the vehicle. Briefly, the loss in the battery voltage causes a reduction in the lift and this necessitates an interpreter between the dynamic model and the controller. We propose a neural network based solution to this problem and this constitutes another, yet equally important, critical contribution of the current study.

This paper is organized as follows: The second section presents the FSMC and related issues. The third section describes the quadrotor dynamics. The fourth section focuses on power loss in the batteries and its compensation utilizing neural networks. In the fifth section, the results obtained through a set of simulations are discussed. Concluding remarks are given at the end of the paper.

II. FRACTIONAL ORDER SLIDING MODE CONTROL SCHEME

Sliding mode control has been a very popular control scheme experimented on various types of dynamic systems admitting switching type control signals, [22]. In this paper, the attractiveness requirement of the sliding subspace is handled.

Consider the dynamic system given as $\ddot{\phi}=f(\phi,\dot{\phi})+\Delta_f+(g(\phi,\dot{\phi})+\Delta_g)u$. In this representation, ϕ and $\dot{\phi}$ are the state variables, $f(\cdot,\cdot)$ and $g(\cdot,\cdot)$ are functions of the state variables referring to the known nominal part, Δ_f and Δ_g denote the unknown but bounded functions of the state variables and time. Besides, u is the input and $g(\cdot)\neq 0$. Consider the reference trajectory for position ϕ_r, which is differentiable, and for velocity $\dot{\phi}_r$. Define the positional tracking error $e_\phi:=\phi-\phi_r$ and its derivative $\dot{e}_\phi:=\dot{\phi}-\dot{\phi}_r$. Let $\ddot{\phi}_r$ denote the second derivative of ϕ_r in terms of time. Based on these variables, set the switching function as $\sigma:=\dot{e}_\phi+\lambda e_\phi$, $\lambda>0$ is the parameter determining the slope of the sliding line. If a control law forces $\sigma=0$ for $t\geq t_0$, then one obtains $e_\phi(t)=e_\phi(t_0)\exp(-\lambda(t-t_0))$, $t\geq t_0$. With a positive valued Q, choosing the reaching law $\dot{\sigma}=-Q\,\mathrm{sgn}(\sigma)$ would force any initial error vector to $\sigma=0$ in finite time as the time derivative of a Lyapunov function $V=\frac{1}{2}\sigma^2$ is negative definite for $\sigma\neq 0$. Calculating the derivative $\dot{\sigma}$ and equating it to $-Q\,\mathrm{sgn}(\sigma)$ then solving for the input (u) yields the control law in (1), where we utilize solely the information about the known nominal part:

$$u=\frac{1}{g(\phi,\dot{\phi})}(\ddot{r}_\phi-Q\,\mathrm{sgn}(\sigma)-\lambda\dot{e}_\phi-f(\phi,\dot{\phi})). \quad (1)$$

Substituting the control law into the system dynamics with uncertainties lets us have

$$\dot{\sigma}=-Q\,\mathrm{sgn}(\sigma)+\Delta_f+\Delta_g u. \quad (2)$$

Clearly if $\sup_{\phi,\dot{\phi},t}|\Delta_f+\Delta_g u|<Q$ then $\sigma\dot{\sigma}<0$ is satisfied and the subspace defined by $\sigma=0$ becomes an attracting subspace making the overall feedback control system insensitive when the error gets trapped to it. It is also possible to derive an upper bound for the time of first hitting to the sliding line, say t_h. In this case, $\dot{e}_\phi=-\lambda e_\phi$ and we have $t_h<\frac{|\sigma(0)|}{Q}$.

When the design presented is considered for the fractional order case, one would proceed as follows. The switching function is chosen as in (3), where Caputo's definition of the fractional order differentiation is given in (4) and Riemann-Liouville definition of which is in (5). In both definitions, $\alpha \in \Re$ and n is an integer, [20].

$$\sigma := e_\phi^{(1+\beta)} + \lambda e_\phi, \quad 0<\beta<1 \tag{3}$$

$$\mathbf{D}^\alpha \phi = \phi^{(\alpha)} := \frac{1}{\Gamma(n-\alpha)} \int_0^t \frac{\phi^{(n)}(\xi)}{(t-\xi)^{\alpha+1-n}} \mathrm{d}\xi \tag{4}$$

$$\mathbf{D}^\alpha \phi = \phi^{(\alpha)} := \frac{1}{\Gamma(n-\alpha)} \left(\frac{\mathrm{d}}{\mathrm{d}t}\right)^n \int_0^t \frac{\phi(\xi)}{(t-\xi)^{\alpha+1-n}} \mathrm{d}\xi \tag{5}$$

where $n-1 \leq \alpha < n$. Choosing the reaching law as given below and evaluating the derivative by using the nominal plant dynamics would let us derive the control law in (7).

$$\sigma^{(1-\beta)} = -Q\,\mathrm{sgn}(\sigma) \tag{6}$$

$$u = \frac{1}{g(\phi, \dot{\phi})} (\ddot{r}_\phi - Q\,\mathrm{sgn}(\sigma) - \lambda e_\phi^{(1-\beta)} - f(\phi, \dot{\phi})) \tag{7}$$

With such a control law, following two questions need to be answered.

- Is it sufficient to deduce the attractiveness of $\sigma = 0$ by only checking $\sigma^{(1-\beta)}\sigma < 0$?
- Is origin the sole attractor of the differential equation given by $e_\phi^{(1+\beta)} = -\lambda e_\phi$?

To understand the attractiveness of the sliding manifold, differentiate (6) to the order $\beta - 1$. Since $\beta - 1 < 0$, this indeed corresponds to fractional order integration, corresponding to negative valued α in Caputo's definition in (4). This lets us have

$$\sigma = -Q\mathbf{D}^{\beta-1}\mathrm{sgn}(\sigma). \tag{8}$$

Differentiating both sides to the order unity yields the equality in (9):

$$\begin{aligned} \dot{\sigma} &= -Q\mathbf{D}(\mathbf{D}^{\beta-1}\mathrm{sgn}(\sigma)) \\ &= -Q\mathbf{D}^{\beta}\mathrm{sgn}(\sigma) \end{aligned} \tag{9}$$

Since $0<\beta<1$, $\mathrm{sgn}(\mathbf{D}^\beta \mathrm{sgn}(\sigma)) = \mathrm{sgn}(\sigma)$ and this leads to the deduction that a control law forcing $\sigma^{(\beta)}\sigma < 0$ would also force $\sigma\dot{\sigma} < 0$. Therefore the control law in (7) renders the subspace defined by $\sigma = 0$ an attractor. To see this, the solution of $\sigma^{(1-\beta)} = -Q\,\mathrm{sgn}(\sigma)$ is obtained for $\sigma(0) = \pm 1$ and $Q = 1$, and $\dot{\sigma}$ is drawn with respect to σ. According to the result, as $|\sigma|$ gets away from the origin, the chosen reaching law creates a stronger push toward the origin. Further, we see that $\sigma\dot{\sigma} < 0$ is satisfied.

According to Caputo's definition in (4) with $n = 1$, one can see that a control law forcing $\sigma^{(\beta)}\sigma = \frac{\sigma}{\Gamma(n-\alpha)} \int_0^t \frac{\dot{\sigma}(\xi)}{(t-\xi)^\beta} \mathrm{d}\xi < 0$ would require opposite signs in σ and $\dot{\sigma}$, which lead to the conclusion $\sigma\dot{\sigma} < 0$. The conclusion of this discussion is that the subspace defined by $\sigma = 0$ is an attractor according to the definition by Caputo.

Similarly, according to the Riemann-Liouville definition of the fractional differentiation in (5) with $n = 1$, obtaining $\sigma^{(\beta)}\sigma < 0$ can arise in the following cases. In the first case, $\sigma > 0$ and the integral $\int_0^t \frac{\sigma(\xi)}{(t-\xi)^\beta} \mathrm{d}\xi$ is monotonically decreasing. In the second case $\sigma < 0$ and the integral $\int_0^t \frac{\sigma(\xi)}{(t-\xi)^\beta} \mathrm{d}\xi$ is monotonically increasing. In both cases, the signal $|\sigma(t)|$ is forced to converge the origin faster than $t^{-\beta}$. A natural consequence of this is to observe a very fast reaching phase as the signal $t^{-\beta}$ is a very steep function around $t \approx 0$.

Regarding the second question, one has to show that the final value of the solution of the fractional order differential equation in (10) is zero.

$$e_\phi^{(1+\beta)} = -\lambda e_\phi, \quad e_\phi^{(\beta)}(t_0) = c_1, \quad e_\phi^{(\beta-1)}(t_0) = c_2 \tag{10}$$

Taking the Laplace transform lets us have $s^{1+\beta} = -\lambda$, which indicates that $\arg(-\lambda) = \pi$ and the condition for stability $\arg(-\lambda) > (1+\beta)\frac{\pi}{2}$ is satisfied. According to [19], $\mathscr{L}(e_\phi(t)) = \frac{c_1 + c_2 s}{s^{1+\beta} + \lambda}$, and clearly the final value theorem will stipulate that $e_\phi(\infty) = 0$ as $c_1, c_2 < \infty$.

Now we focus on how to determine an upper bound for the hitting time, t_h. Under the presence of bounded uncertainties, one would have

$$\sigma^{(1-\beta)} = -Q\,\mathrm{sgn}(\sigma) + \Delta \tag{11}$$

where $0 \leq |\Delta| < M_U < Q$. In analyzing the hitting time, the Riemann-Liouville definition is more useful than Caputo's definition. The analysis is as follows. Utilizing (5) and differentiating (11) to the order β yields

$$\dot{\sigma} = \frac{1}{\Gamma(1-\beta)} \frac{\mathrm{d}}{\mathrm{d}t} \int_0^t \frac{(-Q\,\mathrm{sgn}(\sigma))}{(t-\xi)^\beta} \mathrm{d}\xi \tag{12}$$

which can be rearranged as in (13):

$$\dot{\sigma} = -\frac{Q}{\Gamma(1-\beta)} \frac{\mathrm{d}}{\mathrm{d}t} \int_0^t \frac{\mathrm{sgn}(\sigma(\xi))\mathrm{d}\xi}{(t-\xi)^\beta}. \tag{13}$$

Integrating both sides of (13) from 0 to t_h, and considering the fact that $\mathrm{sgn}(\sigma(\xi))=\mathrm{sgn}(\sigma(0))$ during this interval lets us have

$$\sigma(t_h)-\sigma(0)=-\frac{Q\,\mathrm{sgn}(\sigma(0))}{\Gamma(1-\beta)}\int_0^{t_h} \times\left(\frac{\mathrm{d}}{\mathrm{d}t}\int_0^t\frac{\mathrm{d}\xi}{(t-\xi)^\beta}\right)\mathrm{d}t. \tag{14}$$

After straightforward manipulations and noting that $\sigma(t_h)=0$ yields

$$-\sigma(0)=-\frac{Q\,\mathrm{sgn}(\sigma(0))}{\Gamma(1-\beta)}\int_0^{t_h}\frac{\mathrm{d}\xi}{(t_h-\xi)^\beta}. \tag{15}$$

Solving (15) for t_h gives

$$t_h=\left(\frac{(1-\beta)\Gamma(1-\beta)|\sigma(0)|}{Q}\right)^{\frac{1}{1-\beta}}. \tag{16}$$

Together with the disturbances, it is straightforward to derive the following inequality for the hitting time.

$$t_h\le\left(\frac{(1-\beta)\Gamma(1-\beta)|\sigma(0)|}{Q-M_U}\right)^{\frac{1}{1-\beta}} \tag{17}$$

Briefly, the use of the FSMC law in (7) creates an attracting sliding manifold in the phase space spanned by e_ϕ and $e_\phi^{(1+\beta)}$ and once the error vector falls onto it, the motion thereafter is confined to sliding line. The error and its derivative converge to the origin along the sliding line and the first hitting to the sliding line occurs no later than $(\frac{(1-\beta)\Gamma(1-\beta)|\sigma(0)|}{Q-M_U})^{\frac{1}{1-\beta}}$.

III. QUADROTOR DYNAMICS

Quadrotor type UAVs have been used many times in the past to study the performance of different control schemes. The reason for choosing this particular structure is the fact that its axes fit in the Cartesian coordinate system in such a way that an angular speed change in a rotor causes motion only along one axis. The differential basis of the motion in three dimensional space makes the vehicle dynamics easy to understand and this aspect of the quadrotor configuration motivates us to conduct research on it. The vehicle considered in this study is illustrated in Fig. 1 and the physical parameters

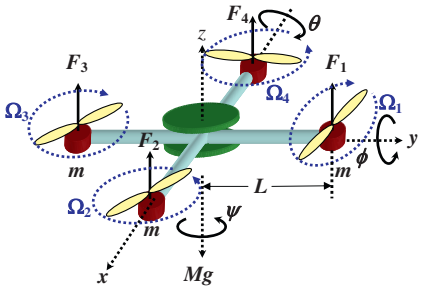

Fig. 1. Schematic view and variable definitions of a quadrotor type UAV.

Table I. Physical Parameters of the Quadrotor UAV.

L	Arm length	0.3 m
M	Mass of the vehicle	0.8 kg
g	Gravitational acc. const.	9.81 m/sec^2
I_{xx}	MoI around x-axis	$15.67e-3$ kg m^2
I_{yy}	MoI around y-axis	$15.67e-3$ kg m^2
I_{zz}	MoI around z-axis	$28.346e-3$ kg m^2
b	Thrust coefficient	$192.3208e-7$ N sec^2
d	Drag coefficient	$4.003e-7$ N m sec^2
j_r	Propeller inertia coef.	$6.01e-5$ kg m^2

are listed in Table I, where MoI is an abbreviation for moment of inertia.

$$\ddot{x}=(\cos\phi\sin\theta\cos\psi+\sin\phi\sin\psi)\frac{1}{M}U_1 \tag{18}$$

$$\ddot{y}=(\cos\phi\sin\theta\sin\psi-\sin\phi\cos\psi)\frac{1}{M}U_1 \tag{19}$$

$$\ddot{z}=-g+\cos\phi\cos\theta\frac{1}{M}U_1 \tag{20}$$

$$\ddot{\phi}=\dot{\theta}\dot{\psi}\left(\frac{I_{yy}-I_{zz}}{I_{xx}}\right)+\frac{j_r}{I_{xx}}\dot{\theta}\Upsilon+\frac{L}{I_{xx}}U_2 \tag{21}$$

$$\ddot{\theta}=\dot{\phi}\dot{\psi}\left(\frac{I_{zz}-I_{xx}}{I_{yy}}\right)-\frac{j_r}{I_{yy}}\dot{\phi}\Upsilon+\frac{L}{I_{yy}}U_3 \tag{22}$$

$$\ddot{\psi}=\dot{\theta}\dot{\phi}\left(\frac{I_{xx}-I_{yy}}{I_{zz}}\right)+\frac{1}{I_{zz}}U_4 \tag{23}$$

where $\Upsilon=\Omega_1-\Omega_2+\Omega_3-\Omega_4$, $U_1=b\Omega_1^2+b\Omega_2^2+b\Omega_3^2+b\Omega_4^2=F_1+F_2+F_3+F_4$, $U_2=b\Omega_4^2-b\Omega_2^2=F_4-F_2$, $U_3=b\Omega_3^2-b\Omega_1^2=F_3-F_1$, $U_4=d(\Omega_1^2-\Omega_2^2+\Omega_3^2-\Omega_4^2)$.

The control problem here is to drive the UAV toward a predefined trajectory in the 3D space by generating an appropriate sequence of Euler angles, which need to be controlled as well. Control of Euler angles is called attitude control and the command signals for Euler angles are produced by the Cartesian

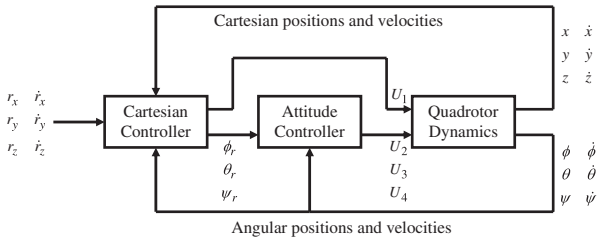

Fig. 2. An overall view of the control system.

controller. The diagram of the control loops are illustrated in Fig. 2, where the variables involved are shown explicitly.

IV. POWER LOSS COMPENSATION USING NEURAL NETWORKS

The dynamical model of a UAV like the one considered in this paper could be obtained using the laws of physics. Principally, a control signal to be applied to the motors must be converted to pulse width modulation signals then electronic speed controllers properly drive the brushless motors. As a result of this, a thrust value is obtained from each motor-propeller pair. The numerical value of the thrust is dependent upon the type of the propeller and the angular speed of the rotor in radians. The relation is given as $F_i = b\Omega_i^2$ where F_i is the thrust at ith motor, b is a constant valued thrust coefficient and Ω_i is the angular speed in rad/sec. If the control inputs (thrusts) needed to observe a desired motion were immediately available, then it would be easier to proceed to the closed loop control system design without worrying about the effects of the actuation periphery. Actuation mechanisms typically introduce some constraints shaping the transient and steady state behavior of the propulsion. Indeed, the real time picture is complicated as the control signals are torques produced by motor-propeller pairs introducing certain transient characteristics. Further, the vehicle here is an electrically powered one, where battery voltage is reducing gradually. Such a change in the battery voltage causes different lift forces at different battery voltage levels although the applied pwm level is constant as seen in Fig. 3. The same 42 second duration pwm profile in Fig. 3 is applied 40 times and as the battery voltage reduces the angular speed at a constant pwm level decreases thereby causing a decrease in the generated thrust. Furthermore, the relation with different pwm levels is not linear, *i.e.* the same amount of change in the input causes different amounts of change at different levels, and this shows that the process to be modeled is a nonlinear one.

According to Fig. 3, comparing the fully charged condition of the battery and the condition at the last experiment displays 15 grams of difference for the lowest level, 154 grams at the highest level, which is obviously an uncertainty that has to be incorporated into the dynamic model and the feedback controller appropriately. Use of neural networks as shown in Fig. 4 is a practical alternative to solve the problem induced by battery conditions. Denoting $V_b(t)$ as the battery voltage, a neural network model performing the map $y_{\text{pwm}} = \text{NN}(\Omega_{i\text{c}}, V_b)$ is the module installed to the output of a controller generating the necessary angular speeds. Here $\Omega_{i\text{c}}$ is the angular speed prescribed by the controller. Another neural network that implements $y_\Omega = \text{NN}(V_b, \text{pwm}, H_2(\text{pwm}))$ is the module installed to the inputs of the dynamic model of the UAV. The box with $H_2(\cdot)$ is a low pass filter incorporating the effect of transience in the thrust value. The dynamic model contains F_is that are computed by using Ω_is.

The reason why we would like to step down from thrusts to the pwm level and step up from pwm level to forces is the fact that brushless DC motors are driven at the pwm level and one has to separate the dynamic model of the UAV and the controller by drawing a line exactly at the point of signal exchange, which occurs at pwm level. Use of neural networks facilitates this in the presence of voltage loss in the batteries.

At this point, it is helpful to describe the pwm scheme briefly. Electronic speed drivers operate at 50 Hz frequency and this corresponds to 20 msec. of period. The lowest level of pwm signal is 0.050, which multiplies 20 msec period and corresponds to 1.1 msec for opening the drivers. The highest level of pwm signal is 0.085, which multiplies 20 msec period to obtain 1.7 msec. Further increase of the duty cycle has no effect on the electronic speed drivers. This discussion shows that a pwm signal having the period 20 msec has the high level in between 1.1 msec to 1.7 msec depending on the pwm signal, and low level in the rest of each period. Needless to say, the pwm signal coefficient is dimensionless as it multiplies the period to yield a quantity in the dimension of milliseconds.

In Fig. 4, the diagram describing the role of the aforementioned offline trained neural models are shown. In Fig. 5, the results obtained with real time data are shown. A chirp like pwm profile was generated and some noise was added to obtain a pwm signal to be applied. When this signal is applied as an input to any motor, the variation in the battery voltage is measured and filtered to guide the neural models as shown in the top right subplot. After that, the corresponding angular

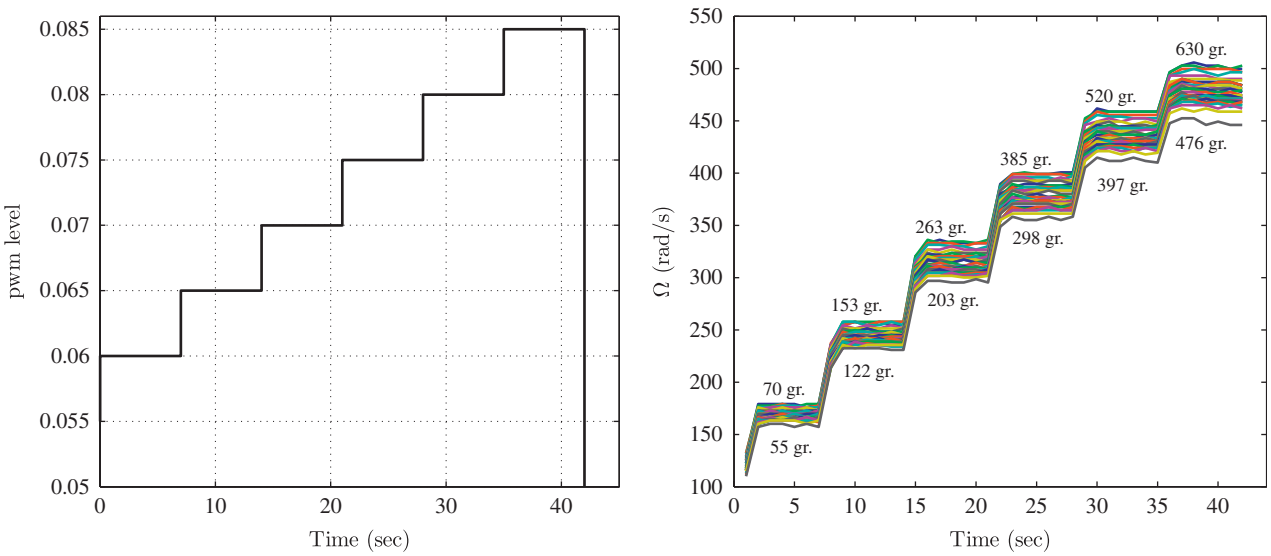

Fig. 3. Left: Applied pwm profile, Right: Decrease in the angular speed as the battery voltage decreases.

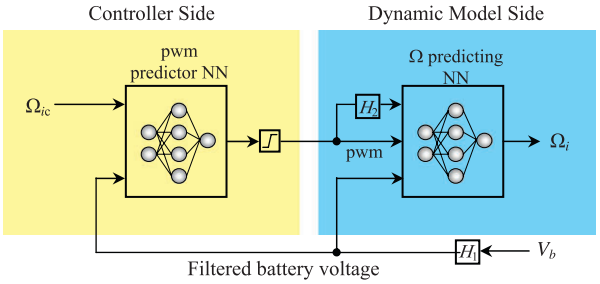

Fig. 4. Installing the neural network components for handshaking at pwm level, whose applicable range is $[0.050, 0.085]$.

speed is computed experimentally. In the middle left subplot, the reconstructed pwm signal and the applied signal are shown together. In the middle right subplot, the performance for the angular speed (Ω) predicting neural model is depicted. Both subplots of the middle row of the figure suggest a useful reconstruction of the signal asked from the neural networks that were trained by using Levenberg-Marquardt algorithm. In both models, the neural networks have single hidden layer with hyperbolic tangent type neuronal nonlinearity and linear output neurons. The pwm predicting model has 12 hidden neurons with a final mean squared error (MSE) value 90.8285×10^{-4}, which is for 88 400 pairs of training data. Angular speed predicting neural model has 10 hidden neurons with a final MSE value 3.9208×10^{-4} for 62 050 pairs of training data collected utilizing a DS1104 data acquisition system.

Bottom subplots of Fig. 5 illustrate the difference between the desired and predicted values. As the local frequency of the target output increases, the neural models start performing more poorly yet the performance is good when the signals change slowly. This is an expected result that is in good compliance with the typical real time signals obtained from a quadrotor type UAV discussed in the previous section.

V. SIMULATION STUDIES

In this section, we describe the Cartesian space controllers producing the command signals for the roll and pitch dynamics and discuss the results of the proposed scheme with a set of simulations.

Denote the reference Cartesian positions and velocities by r_x, r_y, r_z, and $\dot{r}_x$, $\dot{r}_y$, $\dot{r}_z$. We define $P_z := -4\dot{z} - 4(z - r_z)$ and choose the altitude controller as given in (24).

$$U_1 = M \frac{P_z + g}{\cos\theta \cos\phi} \tag{24}$$

Substituting (24) into (18) and (19), and adopting the small angle approximation would let us obtain the dynamics below.

$$\ddot{x} \approx (P_z + g)\tan\theta \tag{25}$$

$$\ddot{y} \approx -(P_z + g)\tan\phi \tag{26}$$

In the above dynamics, $\tan\phi$ and $\tan\theta$ can be regarded as the control inputs for observing the desired motion in Cartesian space. To achieve this, the following

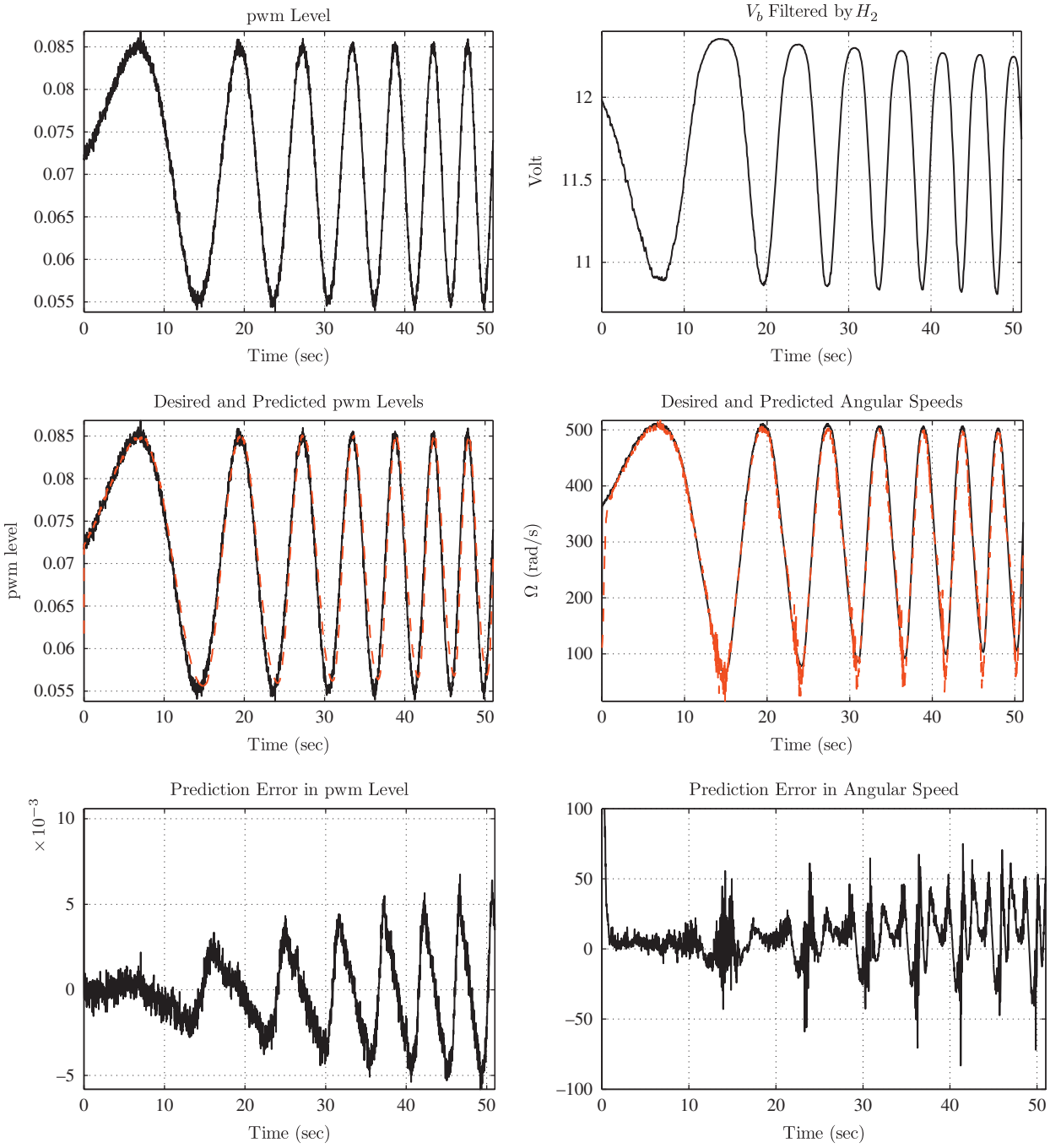

Fig. 5. Performance of the two neural network models.

choices are made:

$$\phi_r = -\arctan\left(\frac{P_y}{P_z+g}\right) \tag{27}$$

$$\theta_r = \arctan\left(\frac{P_x}{P_z+g}\right) \tag{28}$$

where $P_x = -\dot{x} - (x - r_x)$ and $P_y = -\dot{y} - (y - r_y)$. Now we utilize the fractional order sliding mode controller explained in the second section to track these Euler angles to obtain the desired motion. The simulations have been carried out with the settings given in Table II.

Table II. Simulation settings.

β	Frac. differentiation order	0.5
Δt	Simulation stepsize	1 msec.
T	Final time	130 sec.
λ	Slope parameter	0.7
Q	Reaching law parameter	2
δ	Smoothing parameter	0.1
$\phi(0)$	Initial roll	$\frac{\pi}{5}$
$\theta(0)$	Initial pitch	$-\frac{\pi}{6}$
$\psi(0)$	Initial yaw	$-\frac{\pi}{4}$

The other practical considerations implemented are listed below.

- It is a well known fact that sliding mode control systems suffer from the adverse effects of chattering and in the literature, several remedies to this problem have been proposed [23]. The presence of noise and delays in actuation, and the fact that the control signal is dependent upon the sign of a quantity makes the sliding regime display chattering around the sliding manifold. Smoothing the sign function by using $\mathrm{sgn}(\sigma) \approx \frac{\sigma}{|\sigma|+\delta}$ alleviates the chattering effect to some extent yet it introduces a boundary layer thickening the sliding subspace slightly [22].
- In the simulations, we consider a battery discharge profile starting from 11.1 V to 9.9 V in 130 seconds. The voltage levels are determined experimentally with Lithium-Polymer battery packs. The measurements of the battery voltage are affected by the actuation devices adding a bounded and non-periodic high frequency component. Since the neural networks providing the handshaking need as much clear information as possible, filtering of the measurements are inevitable.
- Aside from the initial conditions given in Table II, the remaining set of initial conditions are chosen to be zero, *i.e.* the vehicle is at the origin of the Cartesian space and it is motionless initially. Since the goal is to demonstrate the performance of the proposed fractional order sliding mode control scheme, it is adequate to assume nonzero positional initial values for the Euler angles.
- In order to demonstrate the robustness against disturbances, the angular speeds of the vehicle have been perturbed additively to simulate the effect of weather conditions, such as wind. The perturbations modify the angular speeds to $\Omega_i + K\sin(\frac{2\pi t}{T_i})$, where $T_1 = 10$ sec., $T_2 = 1.2$ sec., $T_3 = 1.8$ sec., $T_4 = 1.27$ sec. and $K = 1$.
- The observations are noisy, the state vector containing the positions and velocities is corrupted by noise sequences of power $1e-6$.
- Another issue to emphasize is the computation of the variable Υ, which is needed in constructing the control law in (7). Notice that the neural network connectivity shown in Fig. 4 has the corrective function at the pwm (physical) level yet tries to match the angular speed claimed by the controller (Ω_{ic}) and its true value (Ω_i). The true value very closely follows the target value and since the controller produces U_1, U_2, U_3 and U_4, we perform the following calculations based on the definitions of U_is.

$$\Omega_{1c} = \sqrt{\frac{1}{4b}U_1 - \frac{1}{2b}U_3 + \frac{1}{4d}U_4} \approx \Omega_1 \tag{29}$$

$$\Omega_{2c} = \sqrt{\frac{1}{4b}U_1 - \frac{1}{2b}U_2 - \frac{1}{4d}U_4} \approx \Omega_2 \tag{30}$$

$$\Omega_{3c} = \sqrt{\frac{1}{4b}U_1 + \frac{1}{2b}U_3 + \frac{1}{4d}U_4} \approx \Omega_3 \tag{31}$$

$$\Omega_{4c} = \sqrt{\frac{1}{4b}U_1 + \frac{1}{2b}U_2 - \frac{1}{4d}U_4} \approx \Omega_4 \tag{32}$$

We assume that the vehicle is equipped with round-per-minute (rpm) sensors that provide a delayed value of the rpm for the relevant rotor. This practically leads to the following expression to predict the value of Υ.

$$\begin{aligned}\Upsilon(t) \approx{}& \Omega_{1c}(t-\tau) - \Omega_{2c}(t-\tau) \\ &+ \Omega_{3c}(t-\tau) - \Omega_{4c}(t-\tau)\end{aligned} \tag{33}$$

where τ is a small delay removing the algebraic loop problems. Though it was possible to choose smaller, in the simulations $\tau = 0.1$ sec has been selected to see how robust the overall control system is.
- Finally, the implementation of fractional order operators need to be discussed. During the simulations, the numerical implementation of the control law in (7) is achieved through the use of well known Crone approximation, which prescribes a series of poles and zeros to build a transfer function $k\prod_{i=1}^{N}\frac{1+s/z_i}{1+s/p_i}$ approximating the desired operator spectrally [24].

In what follows, the simulation results are presented. We consider a trajectory, which is differentiable in all directions of the Cartesian coordinate system. The path followed is depicted in the top left

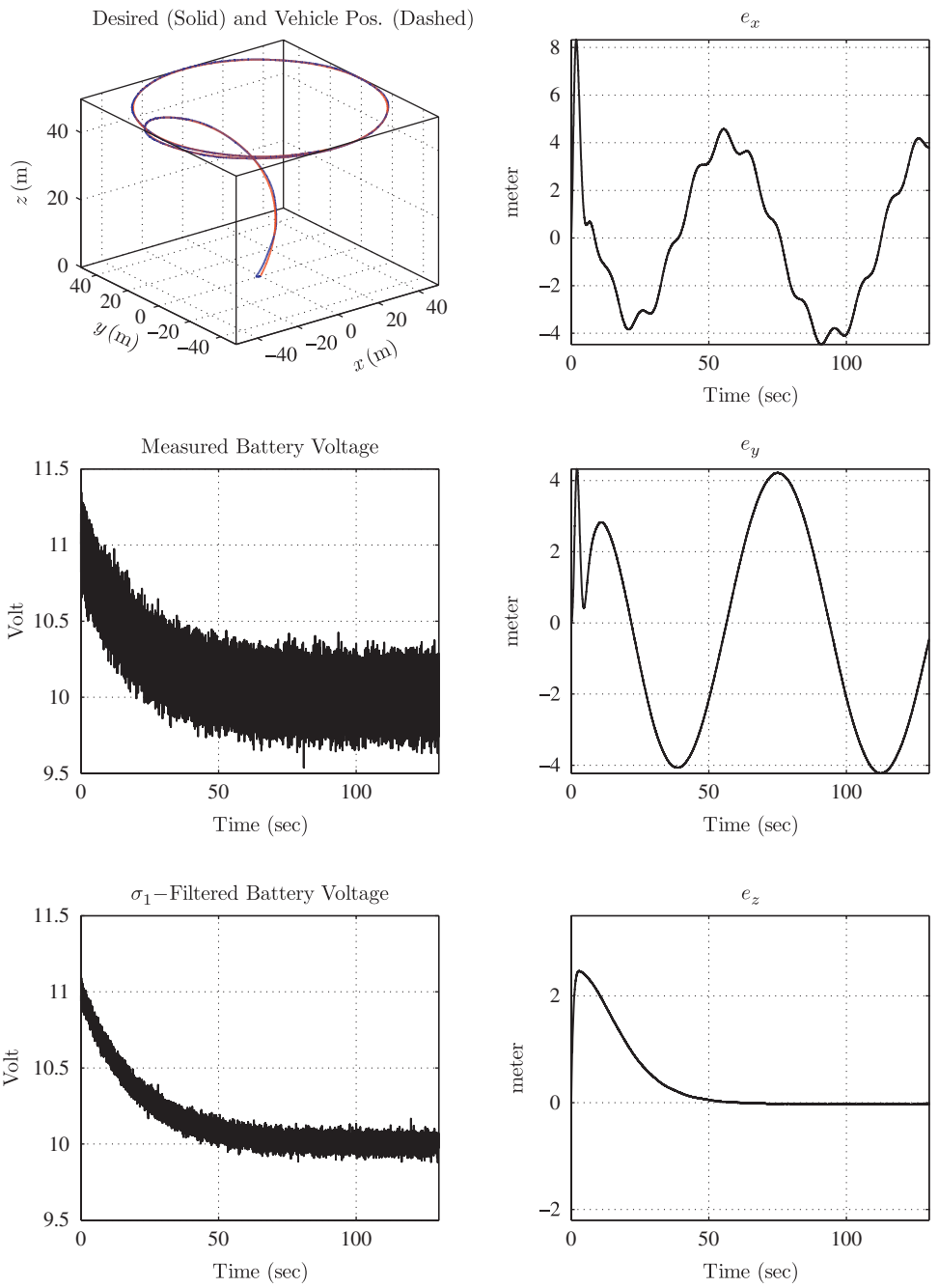

Fig. 6. Cartesian space behavior.

subplot of Fig. 6, where the vehicle is commanded to hover at an altitude of 50 meters and a circular path of radius 50 meters at this altitude is then claimed for tracking. The discharge of the battery is shown in the middle subplot, which displays high frequency fluctuations due to the modulation caused by outrunner brushless motors. The voltage starts from a value of three serially connected Lithium-Polymer battery packs voltage and gradually decreases to the level of 9.9 V in 130 seconds of run. The filtered value of the battery voltage entering the neural models is shown in the bottom subplot. A simple low pass filter, described as $H_1(s)=\frac{10}{s+10}$, is utilized to remove the modulation effect as much as possible and the obtained signal is found acceptable experimentally. The right column of Fig. 6 shows the errors in the Cartesian coordinate

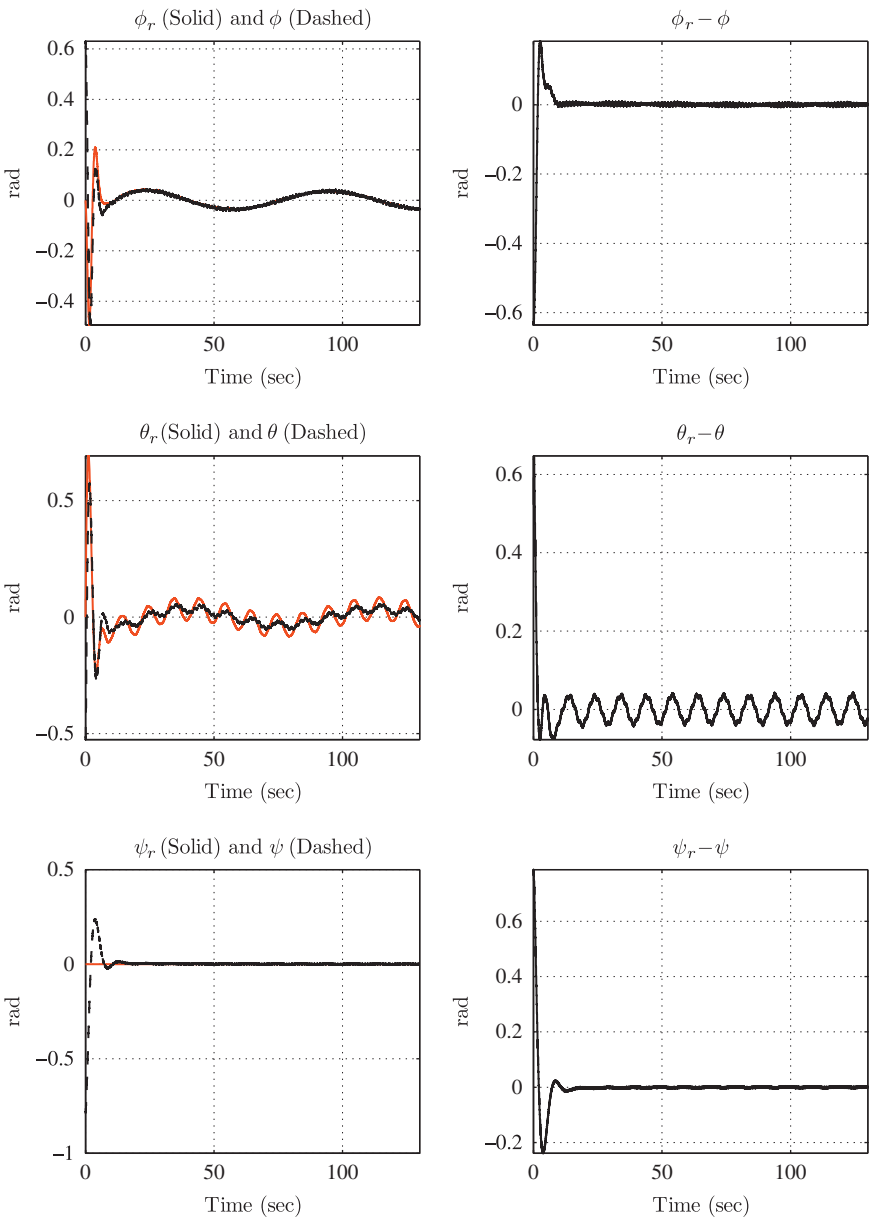

Fig. 7. Vehicle attitude.

system. Comparing the magnitudes with the trajectory shown in the top left subplot, it is seen that the errors observed are tolerable.

In Fig. 7, the attitude, *i.e.* the values of the Euler angles, are illustrated. The Cartesian controller provides the target values of these angles and the fractional order sliding mode controller performs the necessary control signals to be sent to the neural network based module. The left column depicts the evolution of the angles ϕ, θ and ψ respectively, and their target values. After a fast initial transient caused by the initial errors, the prescribed values of the angles are followed accurately as shown also in the error plots in the right column of the figure. The presence of wind disturbances cause fluctuations around the desired trajectory, which is visible in the results seen in Fig. 6.

The phase space behavior is shown in Fig. 8. The left column of this figure depicts the error versus its derivative of order $1+\beta$, and expectedly, we see a quick hitting followed by a sliding regime. The right column of Fig. 8 illustrates the error versus its first (integer) derivative to show what happens in the conventional

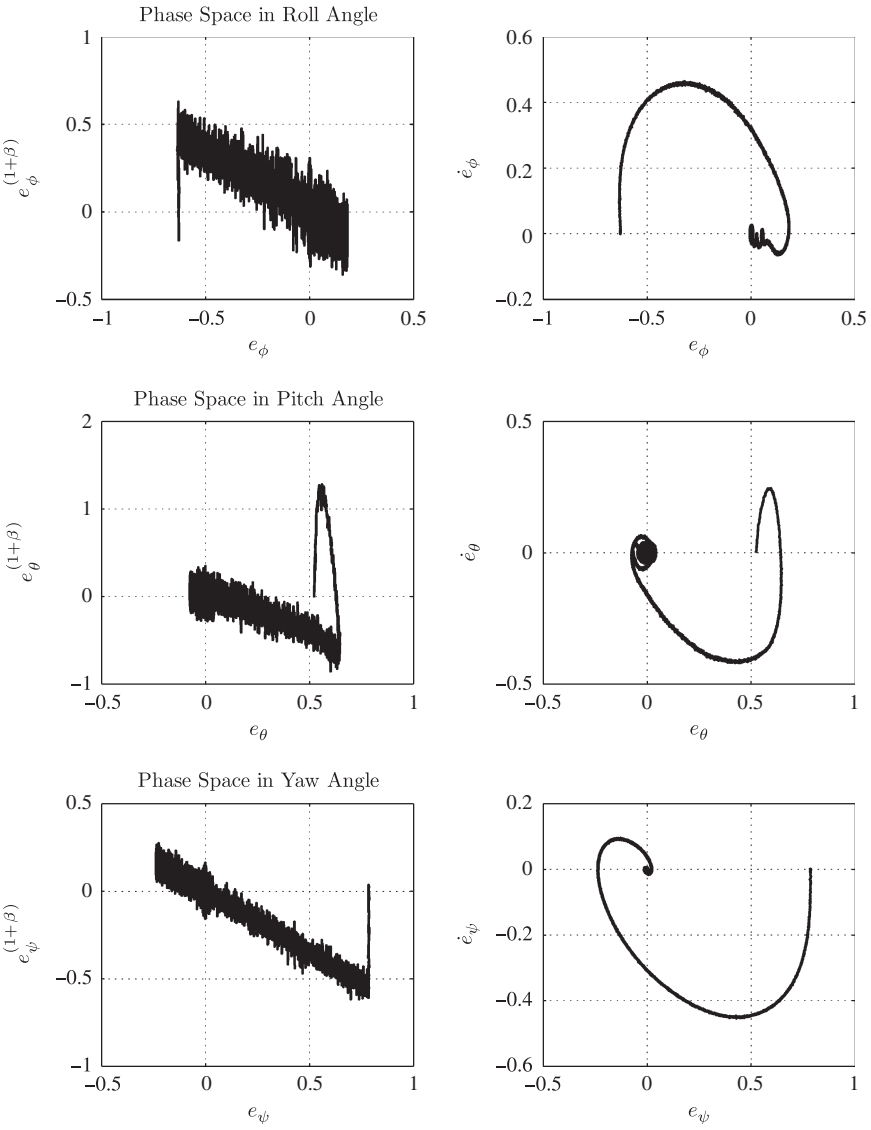

Fig. 8. Phase space behavior.

sense. The path followed in the phase space is convergent, the error and its rate converge to the origin of the phase space in a stable fashion.

The hittings to the switching lines occur at $t_{h,\phi}=0.13$ sec., $t_{h,\theta}=0.25$ sec. and $t_{h,\psi}=0.21$ sec. Due to the influence of measurement noise, use of approximate fractional order operators, the approximation error introduced by the neural networks trained by the use of real time data, and the presence of sign function smoothing, it is difficult to mention a certain value for M_U for each angle but assuming the hitting occurs when $t_h=(\frac{(1-\beta)\Gamma(1-\beta)|\sigma(0)|}{Q-M_U})^{\frac{1}{1-\beta}}$, which corresponds to the worst case, lets us solve an M_U to interpret. With the simulation settings given in Table II, we obtain $M_{U,\phi}=0.5129$, $M_{U,\theta}=1.0882$ and $M_{U,\psi}=0.5262$. Clearly, with these numbers, the proposed controller compensates some amount of uncertainties that reflect the collective effect of the above mentioned issues related to the practice. The difference in the magnitudes of these numbers indicates that the pitch dynamics contain more uncertainty than the roll and yaw dynamics, yet all are robustly compensated to observe the predefined sliding regime after a finite duration of reaching phase.

As a last issue, we compare the performance of the proposed scheme with that of the classical integer order sliding mode controller. We test different levels of disturbances by changing the value of K. Due to the

space limit, results are not presented yet they seem quite promising.

VI. CONCLUDING REMARKS

This paper reports a successful application of fractional order sliding mode control of a quadrotor type UAV, whose dynamic model contains the effect of decrease in the battery voltage. A neural network based compensation of the voltage loss in the batteries is proposed. Neural networks realize the necessary maps providing the handshaking at pulse width modulation signal level, which is the physical border separating the controller and the UAV dynamics containing the effects of motor-propeller pairs. The Cartesian controller is a classical one providing the desired command signals for the Euler angles and the attitude controller is a fractional order sliding mode controller. The paper demonstrates that the sliding manifold is an attractor and the motion taking place on it converges to the origin of the phase space. An upper bound for the hitting time is derived and it is shown via two different flight tests that the derived upper bounds are compatible with the measured ones. Briefly, this paper advances the subject area to the realm of alternatives exploiting the fractional order controllers as well as motion planners considering the battery power conditions efficiently.

REFERENCES

1. Erginer, B. and E. Altug, "Modeling and PD control of a quadrotor VTOL vehicle," *Proc. 2007 IEEE Intell. Vehicles Symp.*, İstanbul, Turkey, pp. 894–899 (2007).
2. Bouchoucha, M., M. Tadjine, A. Tayebi, and P. Müllhaupt, "Step by step robust nonlinear PI for attitude stabilisation of a four-rotor mini-aircraft," *16th Mediterr. Conf. Control Autom.*, pp. 1276–1283 (2008).
3. Mian, A. A. and W. Daobo, "Modeling and backstepping-based nonlinear control strategy for a 6 DOF quadrotor helicopter," *Chin. J. Aeronaut.*, Vol. 21, pp. 261–268 (2008).
4. Kis, L., G. Regula, and B. Lantos, "Design and hardware-in-the-loop test of the embedded control system of an indoor quadrotor helicopter," *Int. Workshop Intell. Solu. Embed. Syst.*, Regensburg, Germany, pp. 1–10 (2008).
5. Cowling, I. D., O. A. Yakimenko, J. F. Whidborne, and A.K. Cooke, "A prototype of an autonomous controller for a quadrotor UAV," *Eur. Control Conf.*, Kos, Greece (2007).
6. Voos, H., "Nonlinear state-dependent Riccati equation control of a quadrotor UAV," *Proc. 2006 IEEE Int. Conf. Control Appl.*, Munich, Germany, pp. 2547–2552 (2006).
7. Waslander, S. L., G. M. Hoffman, S. J. Jung, and C. J. Tomlin, "Multi-agent quadrotor testbed control design: integral sliding mode VS reinforcement learning," *IEEE/RSJ Int. Conf. Intell. Robots Syst.*, Alberta, Canada, pp. 468–473 (2005).
8. Xu, R. and Ü. Özgüner, "Sliding mode control of a class of underactuated systems," *Automatica*, Vol. 44, pp. 233–241 (2008).
9. Tayebi, A. and S. McGilvray, "Attitude stabilization of a four-rotor aerial robot," *43rd IEEE Conf. Decis. Control*, Atlantis, Bahamas, pp. 1216–1221 (2004).
10. Tayebi, A. and S. McGilvray, "Attitude stabilization of a VTOL quadrotor aircraft," *IEEE Trans. Control Syst. Technol.*, Vol. 14, No. 3, pp. 562–571 (2006).
11. Mokhtari, A., and A. Benallegue, "Dynamic feedback controller of Euler angles and wind parameters estimation for a quadrotor unmanned aerial vehicle," *Proc. IEEE Int. Conf. Robot. Automation.*, New Orleans, LA, pp. 2359–2366 (2004).
12. Bouabdallah, S., P. Murrieri, and R. Siegwart, "Design and control of an Indoor Micro Quadrotor," *Proc. IEEE Int. Conf. Robot. Autom.*, New Orleans, LA, pp. 4393–4398 (2004).
13. Guisser, M., H. Medromi, H. Ifassiouen, J. Saadi, and N. Radhy, "A coupled nonlinear discrete-time controller and observer designs for underactuated autonomous vehicles with application to a quadrotor aerial robot," *Proc. 32nd Annu. Conf. IEEE Ind. Electron.*, Paris, France, pp. 1–6 (2006).
14. Guenard, N., T. Hamel, and R. Mahony, "A practical visual servo control for an unmanned aerial vehicle," *IEEE Trans. Robot.*, Vol. 24, No. 2, pp. 331–340 (2008).
15. Bourquardez, O., R. Mahony, N. Guenard, F. Chaumette, T. Hamel, and L. Eck, "Image-based visual servo control of the translation kinematics of a quadrotor aerial vehicle," *IEEE Trans. Robot.*, Vol. 25, No. 3, pp. 743–749 (2009).
16. Kendoul, F., I. Fantoni, and K. Nonami, "Optic flow-based vision system for autonomous 3D localization and control of small aerial vehicles," *Robot. Auton. Syst.*, Vol. 57, pp. 591–602 (2009).
17. Coza, C., and C. J. B. Macnab, "A new robust adaptive-fuzzy control method applied to quadrotor helicopter stabilization," *Annu. Meeting N. Am. Fuzzy Inf. Process. Soc.*, Montreal, Canada, pp. 454–458 (2006).

18. Oldham, K. B., and J. Spanier, *The Fractional Calculus*, Academic Press, New York, NY (1974).
19. Podlubny, I., *Fractional Differential Equations*, Elsevier Science and Technology Books, San Diego, CA (1998).
20. Das, S., *Functional Fractional Calculus for System Identification and Controls*, Springer, Heidelberg, Germany (2008).
21. Ortigueira, M. D., "Introduction to fractional linear systems. Part 1: continuous time case," *IEE Proc. Vis. Image Signal Process.*, Vol. 147, No. 1, pp. 62–70 (2000).
22. Young, K. D., V. Utkin, and Ü. Özgüner, "A control engineer's guide to sliding mode control," *IEEE Trans. Control Syst. Technol.*, Vol. 7, No. 3, pp. 328–342 (1999).
23. Tseng, M. L. and M. S. Chen, "Chattering reduction of sliding mode control by low-pass filtering the control signal," *Asian J. Control*, Vol. 12, No. 3, pp. 392–398 (2010).
24. Valério, D., "Ninteger v. 2.3 Fractional control toolbox for MATLAB," http://web.ist.utl.pt/duarte.valerio/ninteger/ninteger.htm (2005).

Mehmet Önder Efe received his BSc degree from Electronics and Communications Engineering Department, Istanbul Technical University (Turkey) in 1993, and MS degree from Systems and Control Engineering Department, Bogazici University (Turkey), in 1996. He completed his PhD study in Bogazici University, Electrical and Electronics Engineering Department in June 2000. Between August 1996 - December 2000, he was with Bogazici University, Mechatronics Research and Application Center as a research assistant. During 2001, Dr. Efe was a Postdoctoral Research Fellow at Carnegie Mellon University, Electrical and Computer Engineering Department, and he was a Member of the Advanced Mechatronis Laboratory group. Between January 2002 and July 2003 he was with The Ohio State University, Electrical Engineering Department as a Postdoctoral Research Associate. He worked at the Collaborative Center of Control Science. As of September 2003, he started working at Atilim University, Department of Mechatronics Engineering as an Assistant Professor. Dr. Efe was entitled Associate Professor in April 2004 and Full Professor in July 2009. In August 2004, he joined Electrical and Electronics Engineering Department of TOBB University of Economics and Technology. Dr. Efe was the head of the department between August 2004-July 2007 and between June 2008 to August 2010. He has taken several administrative positions at TOBB ETU. Since December 2010, Dr. Efe is with the EEE Department of Bahcesehir University, Istanbul, Turkey. Dr. Efe was the head of IEEE CSS Turkey Chapter between January 2007 and December 2008, and he is currently a Senior Member of IEEE. He serves as an Associate Editor for the journals IEEE Transactions on Industrial Electronics, Transactions of the Institute of Measurement and Control, International Journal of Industrial Electronics and Control and Advances in Fuzzy Systems. Dr. Efe is the author/co-author of more than 120 technical publications focusing on the applications of computational intelligence, unmanned aerial vehicles, and systems & control theory.